Understanding complex magnetic order in disordered cobalt hydroxides through analysis of the local structure

James R. Neilson* and Daniel E. Morse†
Biomolecular Science and Engineering, University of California Santa Barbara, CA 93106, USA

Brent C. Melot, Daniel P. Shoemaker, Joshua A. Kurzman, and Ram Seshadri
Materials Department and Materials Research Laboratory, University of California Santa Barbara, CA 93106, USA

(Received 17 November 2010; revised manuscript received 7 January 2011; published 16 March 2011; publisher error corrected 18 March 2011)

In many ostensibly crystalline materials, unit-cell-based descriptions do not always capture the complete physics of the system due to disruption in long-range order. In the series of cobalt hydroxides studied here, $Co(OH)_{2-x}(Cl)_x(H_2O)_n$, magnetic Bragg diffraction reveals a fully compensated Néel state, yet the materials show significant and open magnetization loops. A detailed analysis of the local structure defines the aperiodic arrangement of cobalt coordination polyhedra. Representation of the structure as a combination of distinct polyhedral motifs explains the existence of locally uncompensated moments and provides a quantitative agreement with bulk magnetic measurements and magnetic Bragg diffraction.

DOI: 10.1103/PhysRevB.83.094418 PACS number(s): 75.25.−j, 61.66.Fn, 64.60.Cn

I. INTRODUCTION

Complex magnetic ground states in crystalline materials frequently derive from the details of the underlying lattices. In the popular example of insulating compounds where the magnetic ions arrange themselves with threefold symmetries (e.g., triangular or pyrochlore lattices), geometric frustration of magnetic interactions prevents magnetic ordering or gives rise to exotic ground states.[1] Alternatively, the dilution of magnetic ions can yield complex magnetic order, since the translational periodicity of the lattice is necessarily interrupted.

For example, in diluted uniaxial anisotropic antiferromagnets, such as $Co_{1-x}Zn_xF_2$, local uncompensated moments result from random variations in the exchange interactions from the nonmagnetic impurities.[2] Upon zero-field cooling, neutron diffraction reveals a Néel state; however, the random fields decrease the diffracted peak intensity from disrupted long-range order (LRO) and field cooling completely destroys the LRO.[3,4] Because these systems show no preference for chemical or short-range order within a disordered nuclear unit cell,[4] it is difficult to structurally distinguish the role of the impurities in establishing the random fields and microdomains.

The layered antiferromagnet, β-$Co(OH)_2$, contains only edge-sharing Co^{2+} octahedra and shows field-induced magnetic behavior below 12.3 K.[5,6] In the α-cobalt hydroxides studied here, the layers of edge-sharing octahedra are disrupted by stellating cobalt tetrahedra (Fig. 1). These modified structures are often referred to as α-$Co(OH)_2$.[7] The series of α-cobalt hydroxide chlorides are described by the chemical formula $Co(OH)_{2-x}(Cl)_x(H_2O)_n$, where $x = 0.2$, 0.3, and 0.4 assumes the tetrahedrally coordinated cobalt content, and $n = 1.3$, 0.9, and 0.3, respectively.[8] We refer to the β-$Co(OH)_2$ compounds as $x = 0$.

In a traditional unit-cell-based description of the structure, all cobalt site occupancies (g) are reduced ($g_{oct} = 1 - g_{tet}$) and randomly averaged [Fig. 1(a)]. Therefore, a local description is needed to locate all of the atom positions and occupancies. From our extensive analysis of the x-ray pair distribution functions of these compounds,[9] the distribution of cobalt polyhedra is best described by a random combination of structural motifs [Figs. 1(b)–1(d)]. We propose that chemical short-range order of the local structure generates complex magnetic behavior, as in diluted uniaxial anisotropic antiferromagnets.

Here we report magnetic susceptibility measurements to reveal uncompensated magnetization, yet magnetic neutron diffraction suggests a periodic Néel antiferromagnetic structure. We present a method of assembling local motifs in real space to microscopically reconcile a quantitative description of the random distribution of exchange interactions and the resulting microdomains.

II. EXPERIMENTAL

The experimental samples with $x = 0.2$, 0.3, and 0.4 were prepared and characterized as previously described[8,9] and material with $x = 0.0$ was purchased from Alfa-Aesar. Magnetic characterization was performed on powder samples embedded in paraffin wax (melted to 55°C) using a Quantum Design MPMS SQUID magnetometer.

The specific heats of $Co(OH)_{2-x}(Cl)_x(H_2O)_n$ for $x = 0.2$, 0.3, and 0.4 and the nonmagnetic analogs $Mg(OH)_2$ and $Zn(OH)_{1.6}Cl_{0.4}H_2O_{0.2}$ were measured using a semiadiabatic technique as implemented in a Quantum Design Physical Property Measurement System. All powder samples were mixed with Ag powder (50 wt.%) in an agate mortar and pestle until homogeneous. Pellets of the mixed powder were pressed in a die (3 mm × 9 mm, ∼0.5 mm thickness) at 0.5 tons. The silver provides mechanical stability to the pellet and improves thermal conductivity to prevent thermal gradients and increase the thermal relaxation. Both stage with thermal grease and Ag calibrations were collected separately before measuring divided pellets (3 mm × 3 mm, approximately 10 mg), which were affixed to the sample stage using thermal grease.

A deuterated analog was synthesized from a D_2O solution for neutron experiments. Neutron diffraction of $Co(OD)_{1.6}(Cl)_{0.4}(D_2O)_{0.3}$ was recorded on the HIPD beamline

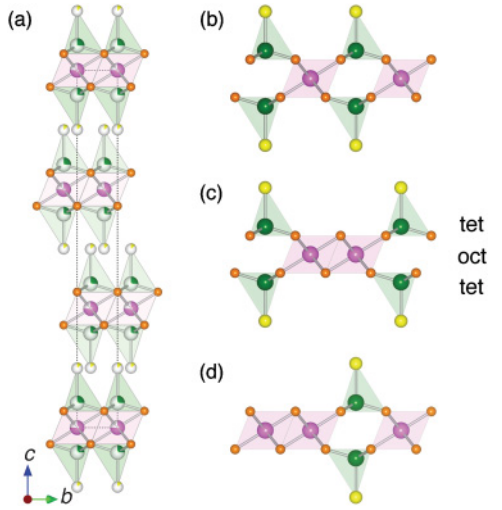

FIG. 1. (Color online) (a) Average structure of layered cobalt hydroxide chloride, $Co(OH)_{2-x}(Cl)_x(H_2O)_n$ (dashed line indicates the unit cell) indicating the fractionally occupied (partially filled) metal sites. (b)–(d) Locally ordered distributions of capping tetrahedral Co^{2+}, with ratios of 2 Co^{tet} per (b) 3 Co^{oct}, (c) 8 Co^{oct}, and (d) 15 Co^{oct}. From Ref. 8. Pink spheres denote Co^{oct}, green Co^{tet}; oxygen is orange, chlorine yellow. Hydrogen is omitted for clarity.

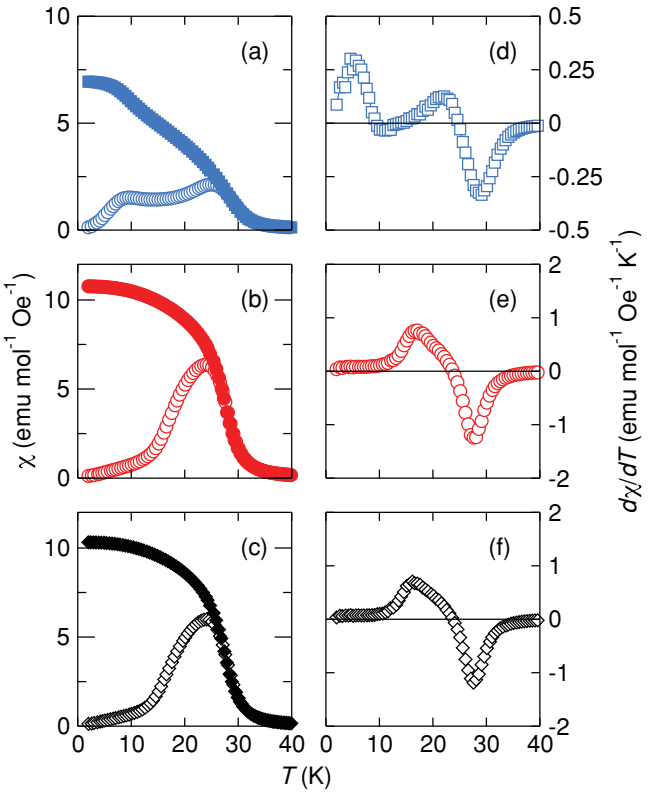

FIG. 2. (Color online) Field-cooled (FC, filled symbols) and zero-field-cooled (ZFC, open symbols) molar dc susceptibility of $Co(OH)_{2-x}(Cl)_x(H_2O)_n$ for $x =$ (a) 0.2, (b) 0.3, and (c) 0.4 for at low temperatures and the temperature derivative of the ZFC curves ($d\chi/dT$) for (d) 0.2, (e) 0.3, and (f) 0.4 indicating two cusps for $x = 0.2$ and an invariant T_c near 24 K. Data acquired under a magnetic field of 100 Oe.

at the Lujan Neutron Scattering Center at Los Alamos National Laboratory at both 6 K and 300 K. Approximately 1 g of sample was packed into a vanadium canister. To calculate and subtract sample absorption using PDFgetN,[10] scattering profiles of the empty vanadium container, the evacuated chamber, and a vanadium rod were also collected. All other experimental details are described in the text where relevant. Experimental uncertainty of reported values (e.g., saturation magnetization, entropy) is determined from the sum in quadrature of fractional uncertainties, with the predominant source of error originating from determination of the measured sample mass.

III. RESULTS AND DISCUSSION

A. Macroscopic magnetization

The static magnetic susceptibilities, measured in zero-field and field-cooling conditions, show a nearly constant T_c with composition, as determined by the temperature at which $d\chi/dT = 0$ (Fig. 2, Table I). The curves for $x = 0.2$ show two cusps at approximately 28.4 K and 9.4 K [Figs. 2(a) and 2(b)], suggestive of multiple ordering transitions or sublattice compensation points. While the lower temperature maximum is obvious for $x = 0.2$, there are subtle changes present in the $x = 0.3$ and 0.4 compounds visible in the ac susceptibility (Fig. 3). All compounds show frequency-dependent cusps in the phase near T_c, and again at ~9 K. The strong frequency dependence in the dynamic susceptibility is supportive of the freezing of glassy spins from different sublattices or microdomains.

From the paramagnetic regime (200 K to 300 K), the inverse susceptibility measured under field cooling is fit to the Curie-Weiss law, $1/\chi = (T - \Theta_{CW})/C$, to extract the constants C and Θ_{CW} (Table I). From data scaled by C and Θ_{CW},

$$\frac{C}{\chi|\Theta_{CW}|} + \mathrm{sgn}(\Theta_{CW}) = \frac{T}{|\Theta_{CW}|}, \quad (1)$$

we compare the relative behavior of all four compounds (Fig. 4). The quality of fit to the Curie-Weiss law is noted by convergence of all data to the ideal Curie-Weiss relationship (dashed black line) at high temperatures in Fig. 4. All of the cobalt hydroxides show strong deflections from the Curie-Weiss law at $T/|\Theta_{CW}| = 1$, indicative of a magnetic phase transition.

All the compounds studied also show small deviations as $T/|\Theta_{CW}|$ approaches unity on cooling. When plotted

TABLE I. Curie temperature determined from $d\chi/dT = 0$ and Curie constants obtained from a linear fit to the Curie-Weiss law from 200 K–300 K.

x	T_c (K)	Θ_{CW} (K)	C (emu mol^{-1} Oe^{-1})
0.0	10.7	14.2	3.1
0.2	24.8, 9.4	31.2	2.0
0.3	23.7	−20.0	2.8
0.4	23.7	−16.9	2.7

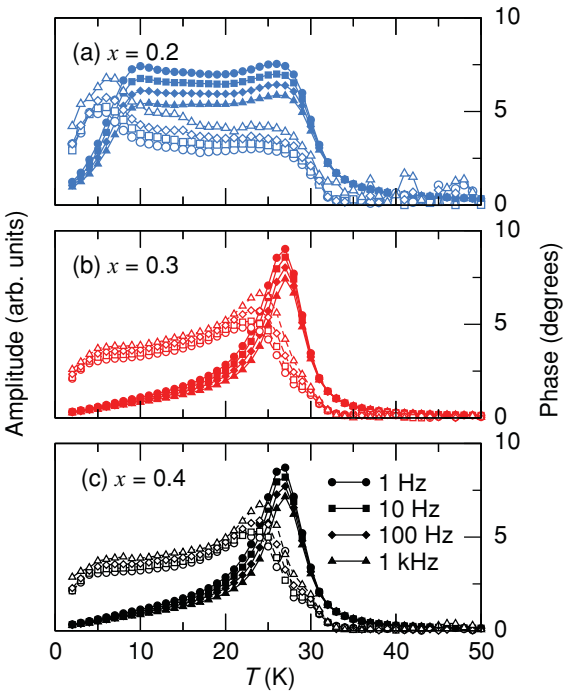

FIG. 3. (Color online) Field-cooled frequency-dependent amplitude (filled symbols) and phase (open symbols) from ac susceptibility measurements of $Co(OH)_{2-x}(Cl)_x(H_2O)_n$ for $x =$ (a) 0.2, (b) 0.3, and (c) 0.4 for low temperatures. Data were acquired with zero applied static magnetic field and an alternating field with an amplitude of 3 Oe.

according to Eq. (1), positive deflections from the ideal Curie-Weiss behavior are indicative of compensated interactions; negative deviations signify uncompensated interactions.[11] The all-octahedral β-$Co(OH)_2$ compound ($x = 0$) shows

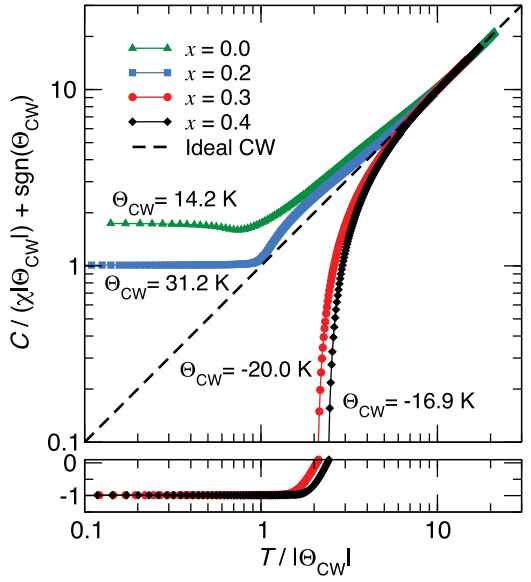

FIG. 4. (Color online) Temperature-dependent scaled inverse susceptibility (field-cooled at 100 Oe) of $Co(OH)_{2-x}(Cl)_x(H_2O)_n$ for $x =$ 0.0, 0.2, 0.3, and 0.4, illustrating positive compensated and negative uncompensated deviations from ideal Curie-Weiss paramagnetism.

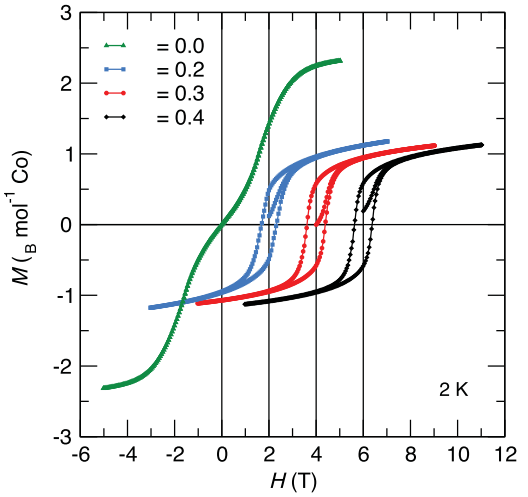

FIG. 5. (Color online) Isothermal magnetization of $Co(OH)_{2-x}(Cl)_x(H_2O)_n$ for $x =$ 0.0, 0.2, 0.3, and 0.4 at 2 K showing the composition independent saturation magnetization for $x > 0.0$. The inflection point in the initial magnetization indicates a weak field induced transition. Each curve is offset by 2 T for clarity.

compensated interactions when $T/|\Theta_{CW}| > 1$, attributable to the longer-range ($\propto r^{-3}$) interlayer dipolar exchange. This is also observed when the layers become decorated with tetrahedra ($x = 0.2$); however, uncompensated interactions emerge when $x > 0.2$. This crossover is reflected in Θ_{CW}, which is positive (ferromagnetic) for $x \leqslant 0.2$, and negative (antiferromagnetic) as $x > 0.2$. As x increases above $x = 0.2$, $|\Theta_{CW}|$ decreases below T_c (Table I), suggesting a decrease in the interaction strength. From a mean-field perspective, we interpret this observation to indicate that the dominant interaction switches from intralayer ferromagnetic coupling when $x \leqslant 0.2$, as found in all octahedrally coordinated cobalt (II) compounds,[12] to antiferromagnetic interactions between distinct polyhedra.

The isothermal magnetization (2 K, Fig. 5) of $x = 0$ is indicative of antiferromagnetic order with a spin-flop transition.[5,12] The hysteresis loops open when $x > 0$ with a composition-independent saturation magnetization at 1.1–1.2 μ_B mol^{-1} Co (Obs. M_{sat} in Table II). This independence contradicts previous studies[13,14] on similar structure types where the Néel sublattices were assigned to

TABLE II. Expected saturation magnetization assuming a two-sublattice Néel model, saturation magnetization for an explicit treatment of the local structure (Ref. 4) and the observed magnetization (2 K,5 T) for each compound ($x = 0.0,0.2,0.3,0.4$). Summary of the magnetic heat capacity measurements: lost entropy and temperature exponent at $T \ll T_c$.

	Néel	Local	Obs.	Heat capacity	
x	M_{sat}	M_{sat} (μ_B mol^{-1} Co)	M_{sat}	ΔS_{mag} (J mol^{-1} K^{-1})	β (T^β)
0.0	n/a	n/a	2.3 ± 0.02	5.2 ± 0.1	2.0
0.2	0.9	1.14 ± 0.07	1.2 ± 0.02	3.7 ± 0.1	1.9
0.3	0.6	1.14 ± 0.07	1.1 ± 0.02	3.6 ± 0.1	2.0
0.4	0.3	1.13 ± 0.07	1.1 ± 0.02	3.4 ± 0.1	2.3

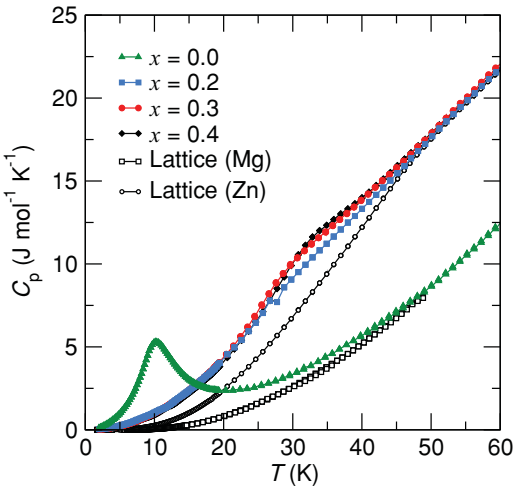

FIG. 6. (Color online) Specific heat capacity measured at low temperature and zero applied field of $Co(OH)_{2-x}(Cl)_x(H_2O)_n$ for $x =$ (a) 0.2, (b) 0.3, and (c) 0.4 and the nonmagnetic analogs $Mg(OH)_2$ and $Zn(OH)_{1.6}Cl_{0.4}H_2O$, after accounting for the differing oscillator masses of the nonmagnetic compounds.

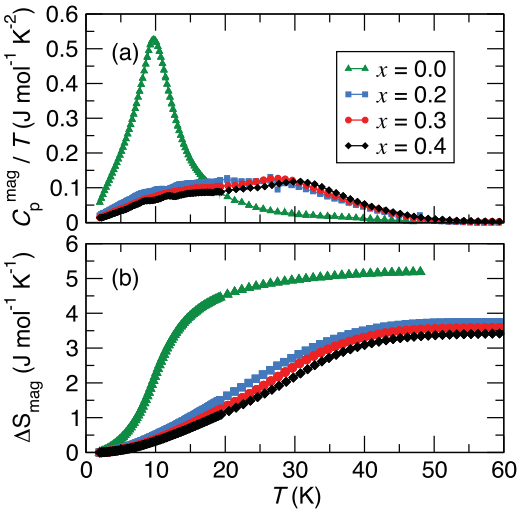

FIG. 7. (Color online) (a) Temperature normalized magnetic heat capacity $[(C_p - C_{\text{lattice}})/T]$ as a function of temperature indicating a broad hump centered around T_c for all compounds. (b) Entropy release through the magnetic ordering transition illustrating the remainder of spin disorder down to 2 K and large entropy losses above the magnetic transition temperature.

different coordination polyhedra (Co^{oct} vs Co^{tet}). Therefore, the expected magnetization is equal to $3/2(Co^{oct}$ sites $- Co^{tet}$ sites). With that spin arrangement, one calculates a composition dependent magnetization (Table II, Néel M_{sat}).

B. Low-temperature heat capacity

Further elucidation of the temperature-dependent magnetism is provided with the magnetic specific heat for each compound, determined using nonmagnetic analogs, $Mg(OH)_2$ for $x = 0$ and $Zn(OH)_{1.6}(Cl)_{0.4}(H_2O)_{0.2}$ for $x > 0$, to subtract contributions from the lattice. To account for the different oscillator masses of the nonmagnetic analogs, their temperature axes were scaled by a ratio of the calculated Debye temperatures (Θ_D) as demonstrated in Ref. 15. The temperature axis of the nonmagnetic analog was divided by the ratio $\Theta_D^{\text{non-mag}}/\Theta_D^{\text{magnetic}}$. The magnetic contribution to the specific heat capacity is then obtained from the algebraic subtraction of the host (nonmagnetic) compound from the experimentally measured specific heat capacity, both illustrated in Fig. 6.

The low-temperature exponents (T^{β},Table II) resemble those of two-dimensional magnetic systems, indicating weak interlayer coupling.[16] There is a significant fraction of entropy lost above T_c, corollary to the observation of short-range spin interactions above the ordering temperature from the Curie-Weiss analysis (Fig. 4). The total entropy lost through the transition is only 25% of the expected value for full ordering of a $S = 3/2$ system $[\Delta S = R\ln(2S + 1)]$ for $x > 0$ (Fig. 7, Table II). Thus, spin disorder persists even at 2 K. Using neutron diffraction, we identify any periodic magnetic order.

C. Neutron diffraction

Magnetic Bragg scattering from time-of-flight neutron powder diffraction of $Co(OD)_{1.6}(Cl)_{0.4}(D_2O)_{0.3}$ ($x = 0.4$; Fig 8) indicates a Néel antiferromagnetic structure. The average magnetic structure, illustrated in Fig. 9(a), describes a spin arrangement with in-plane ferromagnetically coupled spins on octahedral cobalt sites that are antiferromagnetically aligned to adjoining tetrahedral sites. Each layer is antiferromagnetically coupled, yielding a fully compensated magnetic structure, inconsistent with the observed behavior.

To arrive at this result, the unit cell from Ref. 8 was used to initialize the refinement of the nuclear structure at 300 K using FULLPROF.[17] The refinement was simultaneously carried

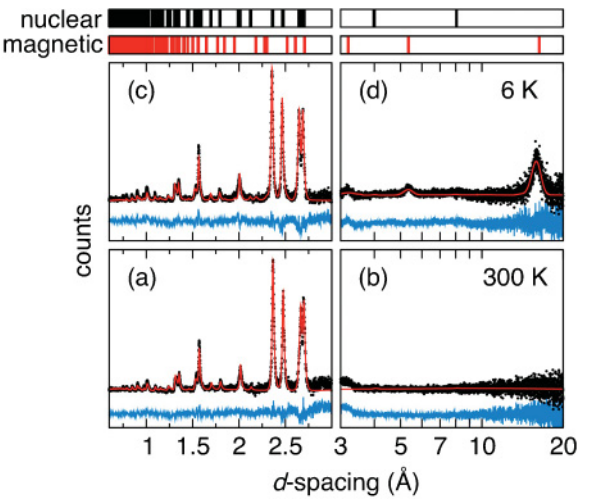

FIG. 8. (Color online) Rietveld refinement of the nuclear and magnetic structures obtained from time-of-flight neutron powder diffraction from the HIPD instrument at [(a) and (b)] 300 K and [(c) and (d)] 6 K for $Co(OD)_{1.6}(Cl)_{0.4}(D_2O)_{0.3}$ with [(a) and (c)] 90° and [(b) and (d)] 14° detector banks, showing the absence of magnetic reflections at large d spacings and a significant contribution of diffuse nuclear scattering at ~3 Å. Expected Bragg planes of the nuclear (black hash marks) and magnetic [red hash marks, $\mathbf{k} = (0,0,1.5)$] phases are shown above, with the Rietveld refined profiles (red lines) above the difference curves (blue lines).

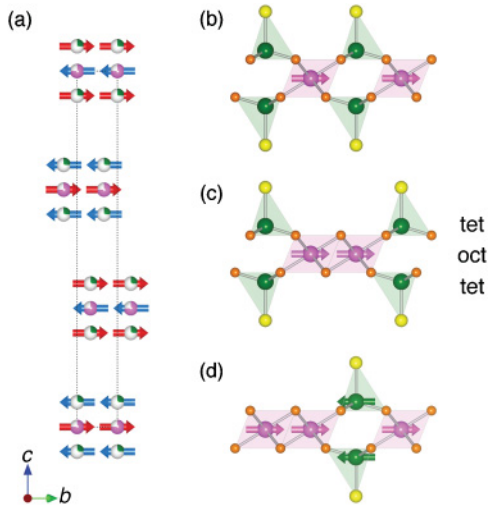

FIG. 9. (Color online) (a) Symmetry-allowed spin configuration of $Co(OD)_{1.6}(Cl)_{0.4}(D_2O)_{0.3}$ at 6 K (dashed line indicates the nuclear unit cell). (b)–(d) Locally ordered motifs (b) $[Co_3^{oct}Co_2^{tet}]$, (c) $[Co_8^{oct}Co_2^{tet}]$, and (d) $[Co_3^{oct}Co_2^{tet}]$ illustrate possible microscopic spin configurations compatible with the average magnetic structure and bulk magnetization. Pink spheres denote Co^{oct}, green Co^{tet}; oxygen is orange, chlorine is yellow, and deuterium is omitted for clarity.

out across multiple time-of-flight detector banks (14°, 40°, and 90°) to achieve a broad range of momentum transfer and resolution, as shown in Figs. 8(a) and 8(b). Deuterium positions were added approximately 1 Å from the μ-(OD) positions and in the interlayer space neighboring the water oxygen position using an equivalent Wyckoff site with twice the occupancy. Both deuterium positions were allowed to refine, along with all other atom positions. The in-plane deuterium and oxygen positions $(x, -x, 0.5)$ are correlated and lead to divergent refinements when unconstrained; therefore, their positions were fixed. The exceptionally high atomic displacement parameters clearly indicate static disorder of the interlayer species and the deuterium bound to μ-(OD) bridging

TABLE III. Structure parameters of $Co(OD)_{1.6}(Cl)_{0.4}(D_2O)_{0.3}$ obtained from Rietveld refinement of data collected at 300 K from time-of-flight neutron powder diffraction, showing fractional coordinates (x,y,z), chemical site occupancies (g), and isotropic atomic displacement parameters (B_{iso}) for a rhombohedral unit cell in a hexagonal setting, $a = 3.142\,66(7)$ Å, $c = 24.037\,38(2)$ Å, $R\bar{3}m$ (166)[a].

Atom	Site	x	y	z	g	B_{iso}
Co(1)	3*a*	0	0	0	0.765	0.2(9)
Co(2)	6*a*	0	0	0.069(5)	0.235	0.2(9)
Cl(1)	6*c*	0	0	0.172(2)	0.235	5.2(9)
O(1)	6*c*	1/3	2/3	0.045(1)	1	2.5(7)
O(2)	18*h*	0.07	0.93	0.5	0.076(5)	1.1(9)
D(1)	6*c*	1/3	2/3	0.080(3)	1	23(9)
D(2)	18*h*	0.4	0.6	0.5	0.15(1)	44(9)

[a]Refinement statistics: 90° bank: $R_p = 4.1\%$, $R_{wp} = 5.6\%$, $\chi^2 = 4.2$; 40° bank: $R_p = 4.2\%$, $R_{wp} = 5.8\%$, $\chi^2 = 2.68$; 14° bank: $R_p = 3.4\%$, $R_{wp} = 4.8\%$, $\chi^2 = 9.1$.

TABLE IV. Basis vectors for the space group $R\bar{3}m$ in a hexagonal setting ($a = 3.136$ Å, $c = 23.928$ Å) with the propagation vector $\mathbf{k} = (0,0,1.5)$. The magnetic representation for the Co^{oct} site, (0,0,0), can be decomposed into the tabulated irreducible representations of $G_{\mathbf{k}}$. The atoms of the nonprimitive basis for Co^{tet} are defined according to 1: (0,0,0.069), 2: (0,0, − 0.069).

			BV components					
IR	BV	Atom	$m_{\parallel a}$	$m_{\parallel b}$	$m_{\parallel c}$	$im_{\parallel a}$	$im_{\parallel b}$	$im_{\parallel c}$
Γ_1	ψ_1	Co^{oct}	0	0	1	0	0	0
Γ_2	ψ_1	Co^{oct}	1	0	0	−0.58	−1.15	0
	ψ_2	Co^{oct}	0	1	0	−1.15	−0.58	0
Γ_1	ψ_1	$Co^{tet}(1)$	0	0	1	0	0	0
		$Co^{tet}(2)$	0	0	1	0	0	0
Γ_2	ψ_1	$Co^{tet}(1)$	1.5	0	0	−0.87	−1.73	0
		$Co^{tet}(2)$	1.5	0	0	−0.87	−1.73	0
	ψ_2	$Co^{tet}(1)$	0	1.5	0	−1.73	−0.87	0
		$Co^{tet}(2)$	0	1.5	0	−1.73	−0.87	0
Γ_3	ψ_1	$Co^{tet}(1)$	0	0	1	0	0	0
		$Co^{tet}(2)$	0	0	−1	0	0	0
Γ_4	ψ_1	$Co^{tet}(1)$	1.5	0	0	−0.87	−1.73	0
		$Co^{tet}(2)$	−1.5	0	0	0.87	1.73	0
	ψ_2	$Co^{tet}(1)$	0	−1.5	0	1.73	0.87	0
		$Co^{tet}(2)$	0	1.5	0	−1.73	−0.87	0

units. The structural parameters of the nuclear structure and refinement statistics are summarized in Table III. Significant diffuse scattering centered around 3 Å (d spacing) is observed at both 300 K and 6 K and also indicates the presence of a large degree of static structural disorder, as previously studied.[8]

The nuclear structure deduced from Rietveld refinement at 300 K was used to initialize the refinement at 6 K. Upon cooling to 6 K, several broad Bragg reflections arise at $d = 3.20$ Å, 5.35 Å, and 16.31 Å [Figs. 8(c) and 8(d)], corresponding to a magnetic propagation vector of $\mathbf{k} = (0,0,1.5)$, commensurate with the nuclear unit cell [$R\bar{3}m$, $a = 3.136$ Å, $c = 23.928$ Å]. Examination of the profile backgrounds does not reveal any additional diffuse scattering at 6 K as evidence for short-range spin correlations.

Using BASIREPS,[18] the irreducible representation (IR) of the Little Group, $G_{\mathbf{k}}$, was decomposed with two unique magnetic atoms (Co^{oct} and Co^{tet}), as summarized in Table IV. The octahedrally coordinated site decomposes into two IR's (Γ_1 and Γ_2). The tetrahedrally coordinated cobalt defines two unique atoms [$Co^{tet}(1)$, $Co^{tet}(2)$] in 4 IR's (Γ_1, Γ_2, Γ_3, and Γ_4). We assume that both cobalt polyhedra belong to the same IR because of intersite connectivity and strong exchange interactions.

Of the allowed IR's, only Γ_2 captures the intensity of the magnetic diffraction peaks. In Γ_2, two basis vectors with real and imaginary components describe the moment contribution on each site. However, powder and domain averaging precludes determination of a unique orientation of the basis vectors within the ab plane of a hexagonal unit cell. Therefore, only the Fourier coefficients (c_{oct}, c_{tet}) of the basis vector ψ_1 within Γ_2 for the Co^{oct} and Co^{tet} sites were allowed to refine. While the cobalt positions are well-defined but partially occupied, refinement to the magnetic reflections reveals partial

spin disorder. The basis vector Fourier coefficients indicate reduced moments of both cobalt sites: 1.2 μ_B for Co^{oct} and 1.1 μ_B for Co^{tet} ($R_{mag} = 14.8\%$, 14° detector bank).

In studies of dilute anisotropic antiferromagnets, magnetic Bragg reflections from quasielastic neutron scattering exhibit increased Lorenztian width from the nuclear reflections and reduced scattering intensity with applied fields.[3,4,19] In those random dilute systems, the formation of magnetic microdomains and the disruption of magnetic long-range order is driven by local random-field energy.[19] While a different experiment here, the magnetic reflections from neutron diffraction have significantly increased Lorenztian widths and low diffracted intensities, which also indicate disrupted long-range order of the magnetic structure. Here, we hypothesize that uncompensated moments from the local clustering of polyhedra disrupt the long-range magnetic order into microdomains, and thus decrease the diffracted intensity and broadens the reflections.

D. Magnetism from local structure

To reconcile ambiguities engendered from fractional occupancy in the unit cell, we refer to our previous local structure study of the pair distribution functions of layered cobalt hydroxide chlorides,[8] depicted in Figs. 1(b)–1(d). We represent the structure from a distribution of $[Co_n^{oct}Co_2^{tet}]$ motifs with a set number of octahedra between tetrahedra. These randomly distributed motifs serve as the microdomains for describing the observed magnetic behavior, redrawn in Fig. 9.

Microscopically, $[Co_{15}^{oct}Co_2^{tet}]$ motifs [Fig. 9(d)] appear as Néel domains, with ferromagnetically coupled octahedral sites, antiparallel to tetrahedral sites, to yield a net local moment. In the $[Co_3^{oct}Co_2^{tet}]$ and $[Co_8^{oct}Co_2^{tet}]$ domains, illustrated in Figs. 9(b) and 9(c), the edge-sharing octahedral sites are ferromagnetically coupled within the layer. However, the tetrahedral sites likely remain disordered, as explained below.

The presence of defect spins, as from tetrahedrally coordinated cobalt sites, often leads to spin disorder. For example, defect spins placed adjacent to well-ordered ferromagnetic layers, as seen in $(1-x)FeTiO_3$-xFe_2O_3 solid solutions,[20–22] results in cluster spin glass behavior. Here, the strong magnetocrystalline anisotropy of octahedral Co^{2+} prevents the canting of spins from the crystal field axes, giving them an Ising character.[23] In the case of high defect concentrations, such as in $[Co_3^{oct}Co_2^{tet}]$ and $[Co_8^{oct}Co_2^{tet}]$ domains, competition between the dominant ferromagnetically coupled layers and the magnetocrystalline anisotropy prevents the formation of a well-ordered ground state. This is supported by the observed trend in decreasing magnetic entropy release with increasing Co^{tet} sites (Table II).

While Goodenough-Kanamori-Anderson superexchange considerations suggest a preference for antiferromagnetic coupling between distinct polyhedra, this interaction is weak, as indicated from the sign change and decreasing $|\Theta_{CW}|/T_c$ with increasing x. On average, a small fraction of tetrahedral spins must align antiparallel to the octahedra, as determined from magnetic neutron diffraction. Disordered tetrahedral spins disrupt the long-range order of interlamellar dipolar coupling, permitting a low-field spin-flop transition. This is observed in the initial magnetization by a change in curvature in $M(H)$ at ~0.4 T (Fig. 5). As the field is reversed, neighboring Néel ordered Co^{tet} spins from distinct layers couple via dipolar interactions along the interlayer space, preventing immediate reversal of the field-induced transition. This gives rise to a remanent magnetization (Fig. 5) and a large frequency-dependent amplitude and phase in $\chi(\omega,T)$ (Fig. 3). While the disparity between the observed magnetization and the fully compensated average Néel antiferromagnetic structure can be reconciled with a spin-flop transition, this cannot account for the nearly composition-independent constant saturation magnetization, T_c, and entropy release. Therefore, a local analysis of the structure must be applied to reconcile these differences.

TABLE V. Summary of local atomic phase fractions from Ref. 8.

x	$[Co_3^{oct}Co_2^{tet}]$ A	$[Co_8^{oct}Co_2^{tet}]$ B	$[Co_{15}^{oct}Co_2^{tet}]$ C
0.2	22%	47%	31%
0.3	29%	51%	21%
0.4	36%	49%	15%

From the polyhedral composition provided by the real-space analysis,[8] we calculate the individual moment contributions from each local motif with the assumption that all Co^{oct} are parallel, and dilute Co^{tet} spins (as in $[Co_{15}^{oct}Co_2^{tet}]$) are antiparallel to Co^{oct} in a Néel configuration [Figs. 9(b)–9(d)]. Letting A, B, and C represent the atomic phase fractions (Table V) of the local motifs provided from Ref. 8 for $[Co_3^{oct}Co_2^{tet}]$, $[Co_8^{oct}Co_2^{tet}]$, $[Co_{15}^{oct}Co_2^{tet}]$, respectively, the summed moment from each microdomain is calculated as

$$M_{sat} = \frac{3}{2}\left(\frac{3A + 8B + (15-2)C}{5A + 10B + 17C}\right). \quad (2)$$

Using Eq. (2), the locally derived saturation moments for $x = 0.2$, 0.3, and 0.4 are tabulated in Table II (local M_{sat}). We compute a negligible dependence of M_{sat} on composition with values comparable to those observed. The agreement of the observed properties with the assembly of local contributions reconciles the inaccuracies resulting from the disordered average structure and microdomain-like magnetic diffraction.

IV. CONCLUSION

While the average symmetry-allowed magnetic structure of the layered cobalt hydroxides appears as a fully compensated Néel-type antiferromagnet, the magnetic behavior is better explained by local and randomly distributed intralayer Néel ferrimagnetic regions that can be aligned with an applied field, interspersed with disordered defect spins that interrupt compensation of the ferrimagnetic regions from layer to layer. We present an extreme case in which magnetic site occupancy exhibits no long-range order, yet a long-range-ordered magnetic structure is observed, on average. Analyses using probes of average structural and magnetic structures are typically interpreted under the assumption that a single unit cell suffices to describe systems in their entirety. This assumption breaks down when there is disorder. We illustrate here that the local atomic structure offers an alternative structural

mechanism for introducing random fields in a magnetic lattice to yield microdomain behavior.

ACKNOWLEDGMENTS

J.R.N. gratefully thanks the NSF for support through the Graduate Research Fellowship. The authors thank A. Llobet, E. E. Rodriguez, and T. M. McQueen for helpful discussions. D.P.S. acknowledges support from the UCSB-LANL Institute for Multiscale Materials Studies. J.A.K. thanks the ConvEne-IGERT Program (NSF-DGE 0801627) for an Associateship. This research was supported by a grant from the DOE, Office of Basic Energy Science, to D.E.M. (DEFG03-02ER46006) and to J.A.K. (DE-FG02-10ER16081); and by use of the time-of-flight beamline HIPD at the DOE's Lujan Center at Los Alamos National Laboratory (operated by Los Alamos National Security, LLC, under the DOE under Contract No. DE-AC52-06NA25396), and UCSB's Materials Research Laboratory (MRL) Central Facilities, supported by the MRSEC Program (NSF, Award No. DMR05-20415), to which B. C. M. also acknowledges financial support; the MRL is a member of the NSF-funded Materials Research Facilities Network (www.mrfn.org).

*neilson@lifesci.ucsb.edu
†d_morse@lifesci.ucsb.edu

[1] A. P. Ramirez, Annu. Rev. Mater. Sci. **24**, 453 (1994).
[2] S. Fishman and A. Aharony, J. Phys. C **12**, L729 (1979).
[3] H. Yoshizawa, R. A. Cowley, G. Shirane, R. J. Birgeneau, H. J. Guggenheim, and H. Ikeda, Phys. Rev. Lett. **48**, 438 (1982).
[4] M. Hagen, R. A. Cowley, S. K. Satija, H. Yoshizawa, G. Shirane, R. J. Birgeneau, and H. J. Guggenheim, Phys. Rev. B **28**, 2602 (1983).
[5] T. Takada, Y. Bando, M. Kiyama, and H. Miyamoto, J. Phys. Soc. Jpn. **21**, 2726 (1966).
[6] X. H. Liu, W. Liu, W. J. Hu, S. Guo, X. K. Lv, W. B. Cui, X. G. Zhao, and Z. D. Zhang, Appl. Phys. Lett. **93**, 202502 (2008).
[7] H. R. Oswald and R. Asper, Bivalent metal hydroxides, in *Preparation and Crystal Growth of Materials With Layered Structures* (D. Riedel Publishing, Boston, 1977).
[8] J. R. Neilson, B. Schwenzer, R. Seshadri, and D. E. Morse, Inorg. Chem. **48**, 11017 (2009).
[9] J. R. Neilson, J. A. Kurzman, R. Seshadri, and D. E. Morse, Chem. Eur. J. **16**, 9998 (2010).
[10] P. F. Peterson, M. Gutmann, T. Proffen, and S. J. L. Billinge, J. Appl. Crystallogr. **33**, 1192 (2000).
[11] B. C. Melot, J. E. Drewes, R. Seshadri, E. M. Stoudenmire, and A. P. Ramirez, J. Phys. Condens. Matter **21**, 216007 (2009).
[12] P. Rabu, S. Angelov, P. Legoll, M. Belaiche, and M. Drillon, Inorg. Chem. **32**, 2463 (1993).
[13] M. Kurmoo, Philos. Trans. R. Soc. London A **357**, 3041 (1999).
[14] M. Kurmoo, Chem. Mater. **11**, 3370 (1999).
[15] A. Tari, *The Specific Heat of Matter at Low Temperatures* (Imperial College Press, London, 2003).
[16] L. P. Regnault and J. Rossat-Mignod, in *Magnetic Propertyies of Layered Transition Metal Compounds*, edited by L. J. de Jongh (Kluwer Academic, Dordrecht, 1990).
[17] J. Rodriguez-Carvajal, Physica B **192**, 55 (1993).
[18] J. Rodriguez-Carvajal, Mater. Sci. Forum **378-381**, 268 (2001).
[19] R. J. Birgeneau, H. Yoshizawa, R. A. Cowley, G. Shirane, and H. Ikeda, Phys. Rev. B **28**, 1438 (1983).
[20] Y. Ishikawa, J. Phys. Soc. Jpn. **17**, 1835 (1962).
[21] Y. Ishikawa, N. Saito, M. Arai, Y. Watanabe, and H. Takei, J. Phys. Soc. Jpn. **54**, 312 (1985).
[22] M. Arai, Y. Ishikawa, N. Saito, and H. Takei, J. Phys. Soc. Jpn. **54**, 781 (1985).
[23] J. Kanamori, Prog. Theor. Phys. **17**, 197 (1957).